JOURNAL OF CATALYSIS 148, 748–758 (1994)

An *in Situ* Infrared Study of the Reactivity of Adsorbed NO and CO on Rh Catalysts

Girish Srinivas, Steven S. C. Chuang,[1] and Santanu Debnath

Department of Chemical Engineering, The University of Akron, Akron, Ohio 44325

Received November 19, 1993; revised April 4, 1994

The reactivity of adsorbed NO and CO has been investigated by combined *in situ* infrared (IR) and mass spectroscopy (MS) on Rh/SiO_2, $Ce–Rh/SiO_2$, and oxidized Rh/SiO_2 at 298–423 K. Exposure of preadsorbed CO to a gaseous NO pulse on Rh/SiO_2, and $Ce–Rh/SiO_2$ resulted in the desorption of linear CO and formation of a low wavenumber NO^- (1650–1700 cm^{-1}) species on the reduced Rh site; exposure of preadsorbed CO on oxidized Rh/SiO_2 to a gaseous NO pulse resulted in the displacement of the gem-dicarbonyl without formation of CO_2 at 298–423 K. Increasing NO exposure time led to the desorption of all adsorbed CO and formation of NO^+ species, a high wavenumber NO^- (1740–1770 cm^{-1}) species, and a bidentate nitrato species. Prolonged exposure of preadsorbed NO to CO resulted in displacement of the adsorbed NO^+ and chemisorption of CO as gem-dicarbonyl and a linear CO on Rh^+. Exposure of the catalyst to a mixture of NO–CO–He (1 : 1 : 3) at 373 K and 0.1 MPa resulted in the formation of CO_2. The formation of CO_2 from the reaction of adsorbed CO with oxygen produced from dissociated NO was more rapid than the desorption of adsorbed CO. The linear CO adsorbed on a Rh site with oxidation state greater than +1 may be a precursor towards CO_2 formation. The increase in the rate of CO_2 formation may be related to the increased coverage and reactivity of adsorbed species in the presence of gaseous NO and CO.

INTRODUCTION

Automobile exhaust is considered one of the largest sources of gaseous pollutants in the world. The main pollutants in automobile exhaust are CO, NO_x, hydrocarbons, particulates, and oxidants. Rh has been successfully used in three-way catalysts to control the emission of NO_x from automobile exhaust, while both Pt and Pd are used as catalysts to oxidize CO and hydrocarbons (1–7). The scarcity and high price of Rh make it desirable to find ways to minimize the Rh content in the catalytic converter. Investigation of the nature and reactivity of adsorbed species on Rh is important to understand the heterogeneous catalytic reaction and could lead toward enhancement in catalyst performance and development of substitutes.

[1] To whom correspondence should be addressed.

Infrared studies have shown that CO chemisorbs on Rh as linear CO and bridged CO on the reduced Rh site and as gem-dicarbonyl on the oxidized Rh site (8–22), the modes of adsorption depending upon the surface state and chemical environment of the catalyst. NO chemisorbs on Rh as a cationic $Rh–NO^+$ species, a neutral NO species, and an anionic $Rh–NO^-$ species (23–30). Infrared (IR) spectroscopy has revealed that the adsorbed NO is the dominant species on the Rh surface with a small coverage of NCO and adsorbed CO during the NO–CO reaction over Rh/SiO_2 at 463–523 K and NO : CO ratio of 1 : 5, and NO conversion below 50% (25, 26). An increase in NO conversion results in an increase in the coverage of adsorbed CO and NCO.

Ce has been an important promoter for the NO–CO reaction (30). The major role of Ce has been identified to be (a) storage of oxygen (31), (b) stabilization of the support and metals (32), (c) promotion of the water-gas shift reaction (33), (d) suppression of N_2O formation (34), and (e) modification of the kinetics of the reaction (34, 35). Ce can be present as either CeO_2 or Ce_2O_3, depending on the gaseous environment of the catalyst surface. The addition of Ce to a Rh/SiO_2 catalyst resulted in an increase in the intrinsic rate constant for CO_2 formation and a decrease in the residence time of intermediates leading to CO_2 formation during the NO–CO (1 : 1) reaction at 573 K (30).

The reactivity and the residence time of adsorbed species depend not only on the composition and state of the catalyst surface, but also on the concentration of the gaseous reactants. The rate of desorption of an adsorbate can be enhanced in the presence of the desorbing species in the gas phase. The rate constant for CO desorption from Ni and Pd has been found to increase with the partial pressure of gaseous CO (36). It is also known that adsorbed CO desorbs from the metal surface in the presence of ^{13}CO, leading to the exchange between adsorbed CO and gaseous ^{13}CO (10, 37). The presence of a gaseous reactant can either promote or inhibit the conversion of adsorbed intermediate to the product (38, 39).

Although previous studies have shown that the interac-

0021-9517/94 $6.00

tion of adsorbed NO and CO can lead to the restructuring of the Rh surface (28, 40, 41), it remains unclear how the presence of gaseous CO and NO alters the reactivity of adsorbed species during the NO–CO reaction. The objective of this work is to investigate the effect of gaseous CO and NO on the reactivity of adsorbed CO and NO on Rh/SiO_2, $Ce–Rh/SiO_2$, and oxidized Rh/SiO_2. The reactivity of preadsorbed CO with NO and that of preadsorbed NO with CO are investigated and compared with the reactivity of the adsorbed species in the presence of gaseous NO and CO. The reactivity of adsorbed species is measured in terms of formation of CO_2. *In situ* IR spectroscopy is employed to monitor the concentration of adsorbed species on the catalysts and mass spectroscopy (MS) is used to determine the composition of the effluents during the pulse experiments and during the steady-state isotopic transient study of the NO–CO reaction.

EXPERIMENTAL

The Rh/SiO_2 catalyst containing 4 wt% Rh was prepared by incipient wetness impregnation of $RhCl_3 \cdot 3H_2O$ (Alfa) onto a silica support (Strem, particle size 70 μm, 350 m^2/g, pore volume 1.7 cm^3/g). An appropriate quantity of $RhCl_3 \cdot 3H_2O$ was dissolved in distilled water to impregnate 1.7 cm^3 of solution into every gram of silica support. The $Ce–Rh/SiO_2$ catalyst containing 5 wt% Rh and 5 wt% Ce was prepared by coimpregnating a solution of $RhCl_3 \cdot 3H_2O$ (Alfa) and $Ce(NO_3)_3 \cdot 6H_2O$ (Alfa) onto the silica (Strem) support. The metal loading of the catalysts was verified by a Philips PV9550 energy dispersive X-ray fluorescence spectrometer. High Rh loading is used to produce the large Rh crystallite so that CO can chemisorb as linear and bridged CO in addition to gem-dicarbonyl. Following impregnation, the catalysts were dried in air overnight at 303 K followed by reduction in flowing H_2 at 673 K for 8 h. The oxidized Rh/SiO_2 catalyst was prepared by oxidizing the reduced Rh/SiO_2 catalyst prior to reaction in flowing air at 673 K for 2 h.

An infrared reactor cell capable of operation up to 873 K and 6 MPa was used for this study (21, 22, 30). The catalysts were pressed into two self-supporting disks (18 mg each); one of the disks was placed in the IR reactor cell and the other one was broken down into flakes and placed at the $\frac{1}{4}$ in. exit line in the immediate vicinity of the infrared beam path. A K-type thermocouple ($\frac{1}{16}$ in. in diameter) is inserted into the IR cell to contact the surface of the catalyst disk. The temperature of the two disks was found to be the same under reaction conditions. The additional catalyst disk was used to increase the amount of desorbing species and conversion to obtain a strong signal in the mass spectrometer. The catalysts were further prereduced in flowing H_2 at 573 K for 2 h or preoxidized in flowing air at 573 K for 2 h, depending on the required conditions of the experiment. The reaction mixture consisted of CO/Ar (custom grade), NO (UHP), and He (UHP), and the gas flows were controlled by mass flow meters. A pulse CO chemisorption study at 303 K showed that the Rh/SiO_2 catalyst chemisorbed 55.3 μmol CO/g catalyst and the $Ce–Rh/SiO_2$ catalyst chemisorbed 28.5 μmol/g catalyst, corresponding to crystallite sizes of 63 and 154 Å, respectively. The number of surface Rh atoms was estimated by assuming CO/Rh = 1 (13). Although it is reported that Ce enhances the dispersion of Rh on Rh/SiO_2 catalysts (35, 42), the lower CO uptake of the $Ce–Rh/SiO_2$ catalyst compared to Rh/SiO_2 in this study could be due to a part of the Rh being covered by Ce.

The system consisted of a pulsing valve capable of introducing a known volume (25 μl) of CO or NO into a He flow to the reactor (43). The residence time of the 25 μl CO pulse in the reactor was 0.85 min. The inlet system also consisted of pulsing and switching valves designed to introduce an abrupt change in the concentration of CO in the form of a ^{13}CO pulse, or a step change from ^{12}CO to ^{13}CO, without disturbing the steady-state flow of the reactants (30, 43). The change in the concentration of adsorbed species during the CO pulse, the NO pulse, and the isotopic transient experiments was monitored by an FTIR spectrometer with a resolution of 4 cm^{-1}. Steady-state spectra were collected using 32 coadded scans and the transient spectra were obtained using 3 coadded scans. The composition of the effluent gas from the IR reactor cell was monitored continuously by a Balzers QMG 112 quadrupole mass spectrometer.

RESULTS

Interaction of NO with Preadsorbed CO on Rh/SiO_2, $Ce–Rh/SiO_2$, and Oxidized Rh/SiO_2

Figure 1 shows the infrared spectra of the interaction of NO with preadsorbed CO on the reduced Rh/SiO_2 at 373 K. CO chemisorption on the reduced Rh/SiO_2 at 0.1 MPa of CO and 373 K, followed by removing the gaseous CO by flushing with He, produced a linear CO band at 2048 cm^{-1} and a bridged CO band at 1900 cm^{-1}. The assignments of these bands agree well with those reported in the literature (8–22). Transient infrared spectra during the first NO pulse showed a gradual decrease in the absorbance of the linear CO and the bridged CO bands with the development of a band due to NO^{-1} at 1675 cm^{-1} (23–30). Three coadded scans used in the transient study yielded infrared spectra with a low signal-to-noise (s/n) ratio. Three coadded scans take approximately 5 s to complete. Increasing the number of coadded scans increases the s/n ratio, resulting in collection of average transient infrared spectra. The higher rate of decrease in the intensity of the linear CO band than in that of the

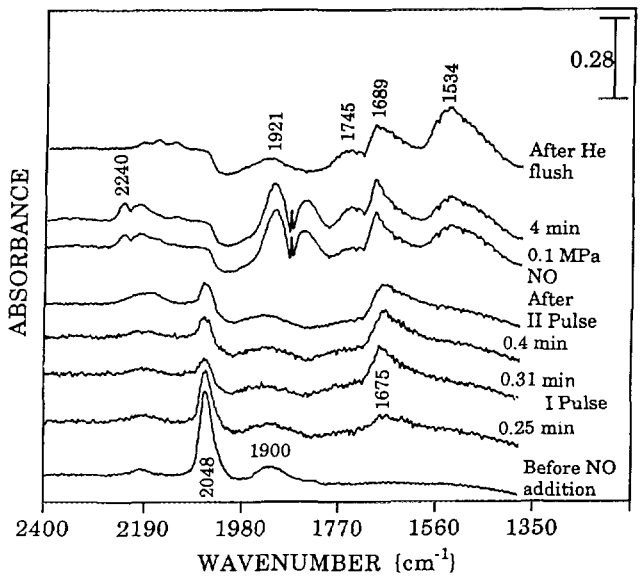

FIG. 1. IR spectra of the interaction of NO with preadsorbed CO on reduced Rh/SiO_2 at 373 K.

bridged CO band indicates that the linear CO is displaced more rapidly than the bridged CO by NO. The spectra obtained after the second NO pulse showed only minor changes. The upward shift in the base line for the spectra above 2000 cm^{-1} during the first NO pulse was due to the slight displacement of the catalyst disk, resulting in incomplete cancellation of the background.

Figures 2A and 2B show the response of effluents from the IR reactor cell during the NO pulses shown in Fig. 1. The *m/e* ratios 28, 30, and 44 correspond to CO, NO, and CO_2, respectively; however, formation of NO–CO reaction products such as N_2 and N_2O could contribute to the *m/e* ratios of 28 and 44, respectively. The first two pulses of NO resulted in near total adsorption of NO, whereas only a part of the NO chemisorbed on the surface during the third pulse, as shown by the breakthrough of NO resulting in a small *m/e* = 30 peak in Fig. 2B. Figures 2C and 2D show the response of an NO pulse through the blank reactor (without the catalyst). The size of the *m/e* = 44 peak during the NO pulse over the catalyst is the same as that of *m/e* = 44 peak during the blank run, suggesting that CO_2 and N_2O were not formed on the Rh/SiO_2 catalyst during the NO pulse over the preadsorbed CO at 373 K, and the reaction

$$NO + CO \rightarrow CO_2 + \tfrac{1}{2} N_2$$

did not occur on the catalyst. The *m/e* = 28 peak observed in Fig. 2A during the NO pulses can be attributed to CO. The decrease in CO, *m/e* = 28, peaks in the successive NO pulses corresponds to the decrease in the extent of CO desorption. Significant CO desorption observed in Fig. 2A compared to little variation of IR spectra during the second NO pulse suggests that most CO observed in the second peak resulted from desorption from the second catalyst disk in the immediate vicinity of the infrared beam path.

Flowing 0.1 MPa of NO over the catalyst resulted in the depletion of the linear and bridged CO bands as shown in Fig. 1 and the development of additional bands at 1921 cm^{-1} due to NO^+, 1745 cm^{-1} due to NO^-, and 1534 cm^{-1} due to bidentate nitrato

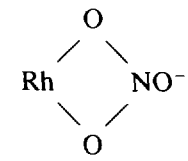

species (23). A weak band at 2240 cm^{-1} is due to gaseous N_2O (44). Flushing the catalyst with He resulted in the removal of the gas-phase NO and N_2O bands with little change in the adsorbed NO bands.

Figure 3 shows the IR spectra of the interaction of NO with preadsorbed CO on $Ce–Rh/SiO_2$ catalyst. The spectra taken before NO addition showed the linear CO band at 2048 cm^{-1}, bridged CO band at 1857 cm^{-1}, the gem-dicarbonyl bands at 2090 and 2027 cm^{-1}, and a tilted CO band at 1766 cm^{-1}. The formation of the tilted CO species is thought to be due to the interaction of the

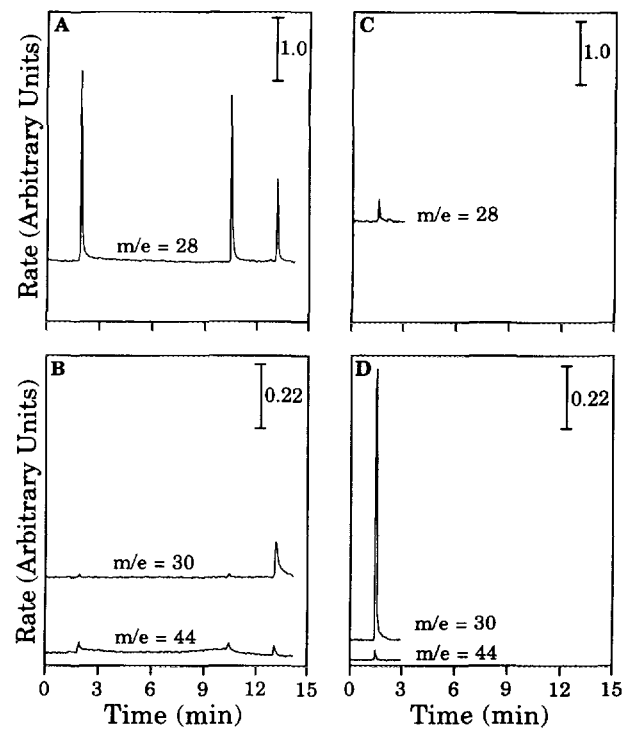

FIG. 2. (A) and (B) MS analysis of the effluents from the reactor for Figure 1. (C) and (D) MS analysis of the effluents from a blank reactor during NO pulses in He.

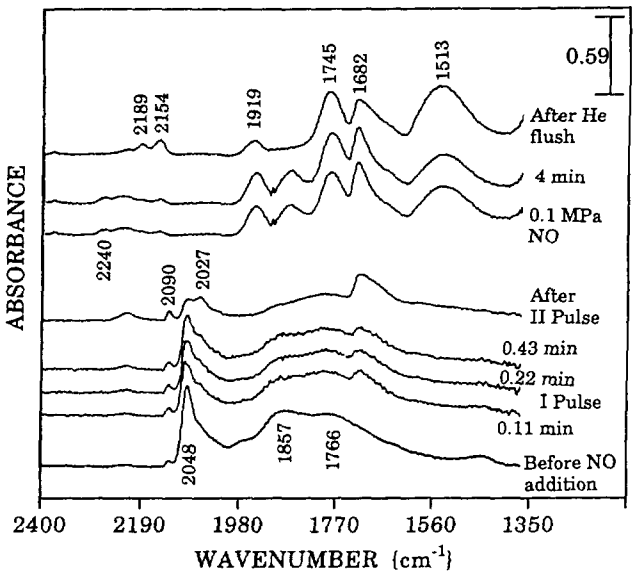

FIG. 3. IR spectra of the interaction of NO with preadsorbed CO on reduced Ce-Rh/SiO_2 at 373 K.

oxygen end of the CO adsorbed on a Rh atom with an adjacent Ce ion (34, 42). It should be noted that tilted CO was observed only on the coimpregnated Ce–Rh catalysts. The tilted CO was not found on the catalyst prepared by sequential impregnation. Coimpregnation appears to maximize the Ce–Rh interface which chemisorbs CO as the tilted CO. IR spectra during the first NO pulse showed that the intensity of the linear CO, bridged CO, and tilted CO bands decreased, while the gem-dicarbonyl bands remained unchanged and a band due to an NO^- species developed at 1682 cm^{-1}. The spectrum following the second pulse showed a further decrease in the intensity of the linear CO band at 2048 cm^{-1}, accompanied by an increase in the intensity of the NO^- band at 1682 cm^{-1}. Flowing 0.1 MPa of NO over the catalyst followed by flushing in He resulted in the depletion of all the adsorbed CO bands with the development of additional bands due to NO^+ at 1920 cm^{-1}, NO^- at 1745 cm^{-1}, and a bidentate nitrato species at 1513 cm^{-1}.

Weak bands at 2154 and 2189 cm^{-1} are due to adsorbed CN and NCO on Rh, respectively (24, 45), while bands at 2240 and 2220 cm^{-1} are due to gaseous N_2O. The mass spectrometer analysis of the effluent from the reactor showed that N_2 and CO_2 were not produced during the NO pulses. The results clearly indicate that the reaction between NO and CO to form CO_2 did not take place. A comparison of the IR spectra during the interaction of NO with preadsorbed CO on Rh/SiO_2 (Fig. 1) and Ce–Rh/SiO_2 (Fig. 3) shows that Ce enhances the formation of bidentate nitrato species on the catalyst at 373 K.

Figure 4 shows the infrared spectra of the interaction of NO with preadsorbed CO on the oxidized Rh/SiO_2 at 373 K. The spectrum obtained prior to pulsing NO over the catalyst displayed strong gem-dicarbonyl bands at 2090 and 2030 cm^{-1} and a band due to linear CO on Rh^+ sites at 2105 cm^{-1}. Pulsing NO over the catalyst resulted in a decrease in the intensity of the gem-dicarbonyl bands and the development of a weak NO^- band at 1682 cm^{-1}. Flowing 0.1 MPa of NO over the catalyst followed by flushing the catalyst with He resulted in the removal of the gem-dicarbonyl species and the development of weak bands due to NO^- at 1752 cm^{-1} and bidentate nitrato at 1520 cm^{-1}. The absence of CO_2 in the effluent indicated that there was no reaction between NO and preadsorbed CO to form CO_2.

Table 1 shows the absolute intensity following CO chemisorption and the percentage of adsorbed CO displaced by the first and second 25 μl pulses of NO on Rh/SiO_2, Ce–Rh/SiO_2, and oxidized Rh/SiO_2 catalyst at 298 K (46) and 373 K (in this study). The values reported in Table 1 are determined by the ratio of intensity of the adsorbed CO displaced after each NO pulse to that before the NO pulse. The percentage of linear CO and bridged CO on Rh/SiO_2 and on Ce–Rh/SiO_2 displaced at 373 K is less than those at 298 K, whereas the percentage of tilted CO on Ce–Rh/SiO_2 displaced at 373 K is greater than that at 298 K. Both linear and bridged CO species desorb on the oxidized Rh/SiO_2 catalyst at 298 K, while the only chemisorbed CO observed on the oxidized Rh/SiO_2 catalyst at 373 K is the gem-dicarbonyl species, which is displaced by NO. The negative values reported for gem-dicarbonyl on the Ce–Rh/SiO_2 catalyst at 373 K shown in Table 1 are due to enhancement in intensity of the gem-dicarbonyl bands by conversion of a part of the linear, bridged, or tilted CO to gem-dicarbonyl during the NO

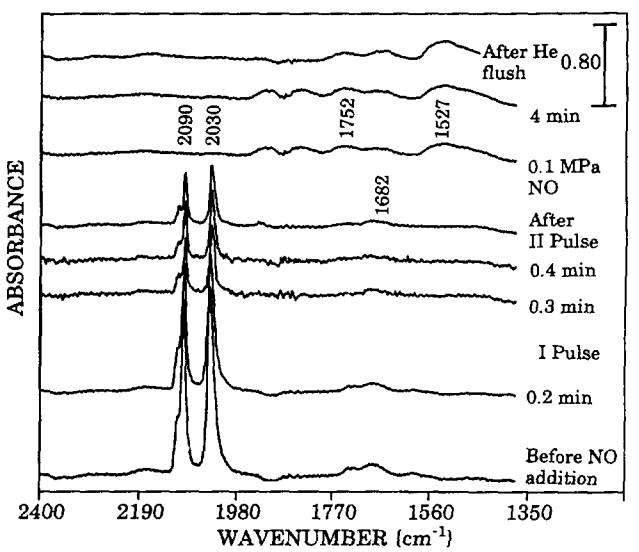

FIG. 4. IR spectra of the interaction of NO with preadsorbed CO on oxidized Rh/SiO_2 at 373 K.

TABLE 1

Percentage of Adsorbed CO Displaced during NO Pulses

Pulse	Rh/SiO_2					$Ce–Rh/SiO_2$							Oxidized Rh/SiO_2					
	298 K			373 K		298 K			373 K				298 K			373 K		
	L	B	G	L	B	L	B	T	L	B	G	T	L	B	G	L	B	G
A_I^a	0.15	0.06	0.04	0.18	0.04	0.44	0.34	0.23	0.50	0.35	0.05	0.33	0.62	0.34	0.75	—	—	1.50
I	66	66	20	56	20	57	12	9	33	33	−25	21	36	23	3	—	—	65
II	14	64	25	9	25	76	21	9	56	49	−50	36	37	68	4	—	—	14

Note. Legend: L, linear CO; B, bridged CO; G, gem-dicarbonyl; T, tilted CO.
[a] Initial intensity (arbitrary units).

pulses. It should be noted that the presence of gem-dicarbonyl on both reduced Rh and Ce–Rh at 298 K is a result of CO-induced disruption of Rh crystallites (17).

Interaction of CO with Preadsorbed NO on Rh/SiO_2 and $Ce–Rh/SiO_2$

Figure 5 shows the IR spectra of the interaction of CO with preadsorbed NO on Rh/SiO_2 at 373 K. The Rh/SiO_2 catalyst was exposed to 0.1 MPa of NO for 5 min, followed by removal of the gaseous NO by flushing with He. The spectrum obtained prior to pulsing CO showed the NO^+ band at 1904 cm^{-1}, the NO^- bands at 1740 and 1655 cm^{-1}, and the bidentate nitrato band at 1530 cm^{-1}. Pulsing CO over the catalyst did not result in any change in the intensity of the adsorbed species and no gaseous NO was detected in the effluent of the reactor. Flowing 0.1 MPa of CO followed by flushing the catalyst with He resulted in the gradual decrease in the intensity of all the adsorbed NO bands with the slow development of the gem-dicarbonyl bands at 2093 and 2038 cm^{-1}, and a shoulder band at 2105 cm^{-1} due to a linear CO species on Rh^+ sites (21, 22). A band observed at 2160 cm^{-1} is due to adsorbed CN on Rh. Comparison of the response of m/e = 28, 30, and 44, corresponding to CO, NO and CO_2 in the effluent to those during a pulse through the blank reactor (without the catalyst) showed that reaction of adsorbed NO with CO to form N_2 and CO_2 did not take place.

The interaction of CO with preadsorbed NO on $Ce–Rh/SiO_2$ was investigated and the IR spectra during the experiment are shown in Fig. 6. The spectrum obtained prior to the introduction of CO showed the NO^+ band at 1909 cm^{-1}, the NO^- bands at 1746 and 1655 cm^{-1}, and the bidentate nitrato band at 1517 cm^{-1}. Pulsing CO sequentially to the catalyst did not result in any changes in the bands due to adsorbed NO but led to the development of

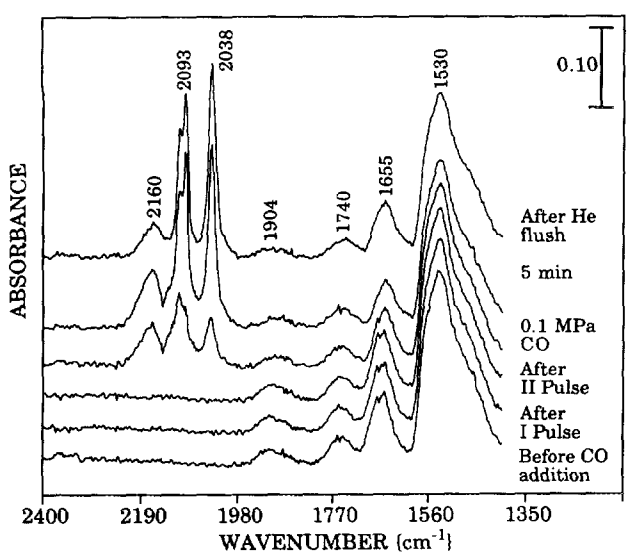

FIG. 5. IR spectra of the interaction of CO with preadsorbed NO on reduced Rh/SiO_2 at 373 K.

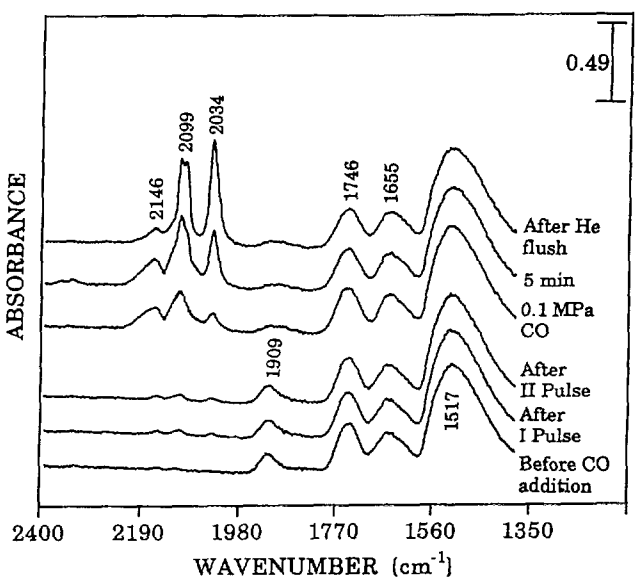

FIG. 6. IR spectra of the interaction of CO with preadsorbed NO on reduced $Ce–Rh/SiO_2$ at 373 K.

weak gem-dicarbonyl bands at 2099 and 2034 cm^{-1} and a weak CN band at 2146 cm^{-1}. Flowing 0.1 MPa of CO on the catalyst resulted in a decrease in the intensity of the NO^+ band at 1909 cm^{-1} and a gradual increase in the intensities of the gem-dicarbonyl and CN bands and a band due to Rh^+ (CO) at 2105 cm^{-1}, while the NO^- and bidentate nitrato bands decreased only slightly in intensity. The greater decrease in the intensity of the NO^+ band than those of the NO^- and bidentate nitrato bands indicates that the NO^+ species is displaced at a higher rate by CO than the NO^- and bidentate nitrato species. No reaction products were detected in the effluent from the reactor during the pulses similar to that on the Rh/SiO_2 catalyst.

An attempt was made to investigate the interaction of CO with preadsorbed NO on oxidized Rh/SiO_2 at 373 K; however, no adsorbed NO bands were detected even after prolonged exposure of the catalyst to 0.1 MPa NO. Admitting CO to the catalyst resulted in the gradual development of gem-dicarbonyl bands on the catalyst (46). An MS analysis of the effluent gases showed that there was no reaction between adsorbed NO and CO to form CO_2 and N_2.

Interaction of NO with Preadsorbed ^{13}CO on Rh/SiO_2

Interaction of adsorbed CO with NO was investigated at 423 K to determine the effect of temperature on the reactivity of adsorbed species. Figure 7 shows the IR spectra of the interaction of NO with preadsorbed CO on Rh/SiO_2 at 423 K. CO was first chemisorbed on Rh/SiO_2 at 473 K by pulsing 25 μl of CO in He to investigate the reactivity of NO with the adsorbed CO; however, the rapid desorption of CO and conversion of CO to CO_2 at

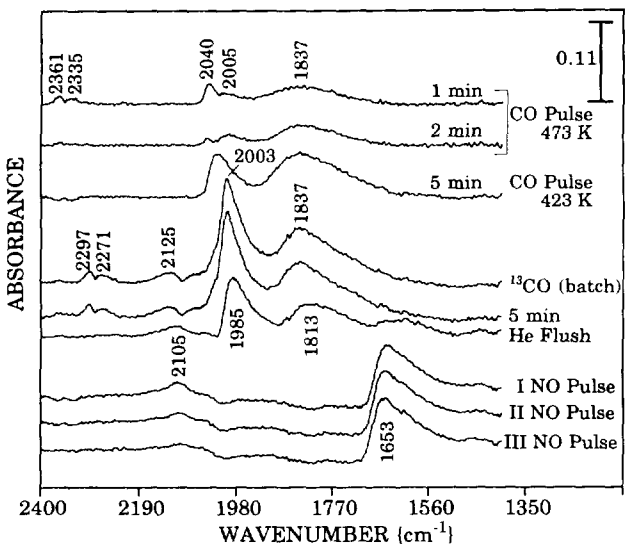

FIG. 7. IR spectra of the interaction of NO with preadsorbed CO on reduced Rh/SiO_2 at 423 K.

473 K led to the removal of almost all the linear (2040 cm^{-1}) and bridged (1837 cm^{-1}) CO on the catalyst in 2 min. Bands at 2361 and 2335 cm^{-1} are due to the formation of CO_2 during the CO pulse. CO was then pulsed at 423 K. The intensity of the linear (2030 cm^{-1}) and bridged CO (1837 cm^{-1}) species decreased and leveled off after 5 min, as shown in Fig. 7. The adsorbed CO was exchanged with ^{13}CO before investigating its interaction with NO, which provided a method for decoupling the contributions from N_2 to CO and from N_2O to CO_2 in the MS analysis.

Admitting 10 cm^3 of ^{13}CO into the reactor and keeping the outlet of the reactor closed resulted in the following changes in the IR spectra: (i) the development of bands at 2297 and 2271 cm^{-1} due to $^{13}CO_2$ and at 2125 cm^{-1} due to gaseous ^{13}CO, (ii) a rapid disappearance of the linear CO band at 2030 cm^{-1} with the formation of a linear ^{13}CO band at 2003 cm^{-1}, and (iii) a small enhancement in intensity of the band at 1837 cm^{-1}. A comparison of the rate of exchange of the linear and bridged CO with gaseous ^{13}CO shows that the linear CO exchanges with gaseous ^{13}CO rapidly while little exchange of bridged CO is observed at 423 K under the batch conditions. Flushing the catalyst with He resulted in a decrease in the intensity and wavenumber of the linear ^{13}CO band and the band at 1837 cm^{-1}. The weak band at 2105 cm^{-1} is assigned to linear ^{13}CO on Rh^{2+} or Rh^{3+} sites. Exchange of adsorbed ^{13}CO (linear, bridged, and gem-dicarbonyl) with gaseous ^{12}CO has been reported on Rh/Al_2O_3 at 298 K (10). The reason for the slow exchange of the bridged CO with gaseous ^{13}CO in this study remains unknown.

Pulsing 25 μl of NO to the reactor resulted in almost total desorption of the linear (1985 cm^{-1}) and bridged (1813 cm^{-1}) ^{13}CO with an increase in the intensity of the 2105 cm^{-1} band, and the development of the NO^- band at 1653 cm^{-1}. Subsequent pulses of NO to the catalyst resulted in decreases in intensity of all the adsorbed CO bands and a small increase in the intensity of the NO^- band. The increase in the intensity of the 2105 cm^{-1} band after the first NO pulse could be due to conversion of part of the linear or bridged ^{13}CO on Rh^0 sites to the linear ^{13}CO species on Rh^{2+} or Rh^{3+} sites.

Figure 8A and 8B show the response of ^{13}CO, NO, $^{13}CO_2$, N_2, and N_2O with m/e = 29, 30, 45, 28, and 44, respectively, in the effluent of the IR reactor cell during the NO pulses shown in Fig. 7. Successive NO pulses resulted in the decrease in the area under the m/e = 29 response, while the area under the successive m/e = 30 peaks increased and remained constant after the fourth pulse. The linear and bridged ^{13}CO species exhibiting the 1985 and 1813 cm^{-1} bands were removed almost completely during the first pulse. The gaseous ^{13}CO species desorbing from the catalyst, corresponding to the area under the second and third m/e = 29 peaks, is due to the desorption of the linear ^{13}CO species on Rh^{2+} (or Rh^{3+})

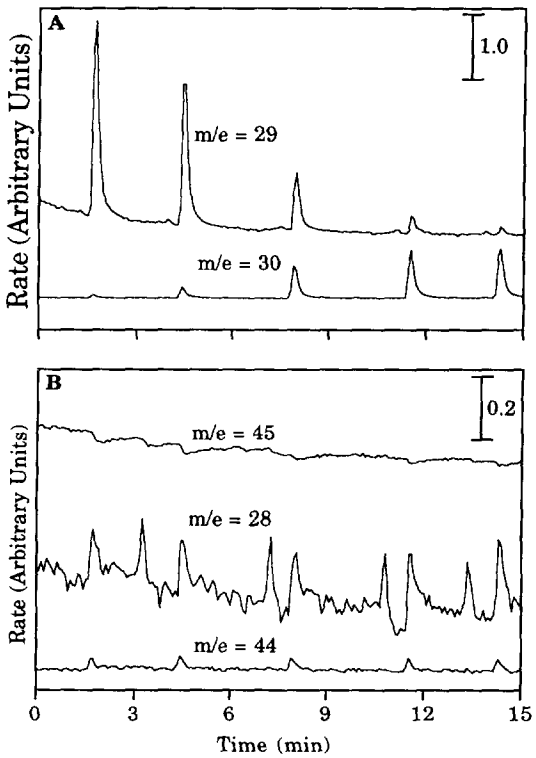

FIG. 8. MS analysis of the effluents from the reactor for Fig. 7.

at 2105 cm^{-1} and adsorbed CO from the second catalyst disk located at the exit line of the reactor. Almost all the adsorbed ^{13}CO was displaced by NO after the fourth pulse. Examination of the $m/e = 45$ response showed that $^{13}CO_2$ was not formed during the pulses. Comparison of the $m/e = 28$ and 44 responses during the pulses to those during NO pulses through the blank reactor, shown in Figs. 2C and 2D, revealed that little N_2 and N_2O was produced during the NO pulses over the catalyst.

Steady-State Isotopic Investigation of NO–CO Reaction on Rh/SiO_2 and $Ce–Rh/SiO_2$

Investigation of the effect of gaseous NO and CO on the reactivity of adsorbed species during the NO–CO reaction was undertaken by steady-state isotopic analysis of the NO–CO reaction on Rh/SiO_2 and $Ce–Rh/SiO_2$ at 373 K. The studies were undertaken by pulsing 10 cm^3 of ^{13}CO into a steady-state flow of ^{12}CO while maintaining the ratio of $^{12}CO : NO = 1 : 1$ during the isotopic experiment. Helium was used as an inert diluent in the reaction mixture and 2% Ar was used in the ^{12}CO stream as a tracer to determine the dynamics of the reactant flow in the reactor and transportation lines. Figure 9 shows the normalized MS response, $E(t)$, during the isotopic pulse study on Rh/SiO_2 at 373 K (30, 43). The negative ^{12}CO response resembles the mirror image of the positive ^{13}CO response suggesting that the total ^{12}CO and ^{13}CO flow was maintained nearly constant and an approximately equal amount of ^{12}CO was replaced by ^{13}CO during the pulse transient. Since ^{13}CO has the same chemical properties as ^{12}CO, the chemical environment of adsorbed species was not disturbed by the ^{13}CO pulse. The $^{13}CO_2$ response led that of ^{13}CO. The average residence time, τ, of adsorbed species and intermediates leading to gaseous species was calculated from Fig. 9 by the relation (47)

$$\tau = \frac{\int_0^\infty tE(t)dt}{\int_0^\infty E(t)dt}.$$

The actual residence times (τ) for ^{13}CO and $^{13}CO_2$ on the catalyst surface were calculated by subtracting the τ for Ar, which denotes the residence time of the gaseous reactant through the reactor and transportation lines.

Figure 10 shows the IR spectra during the isotopic pulse transient on Rh/SiO_2. The low signal-to-noise ratio results from the use of three coadded scans for the collection of transient infrared spectra. The spectrum obtained prior to pulsing ^{13}CO showed a prominent CN band at 2160, bands due to NO^+ species at 1917 cm^{-1} and NO^- species at 1767 and 1683 cm^{-1}, a band due to bidentate nitrato species at 1528 cm^{-1}, and a CO band at 2128 cm^{-1}. The adsorbed CO species exhibiting a 2116–2120 cm^{-1} band has been assigned to a linear CO on a Rh^{2+} site (11). The CO band observed near this region is tentatively assigned to the linear CO on the Rh^{2+} site. The assignments of the other carbonyl (8–22), cyanide (45) and nitrosyl (23–30) bands are well documented in the literature. The spectrum of the gaseous NO–CO–He($NO : CO : He = 1 : 1 : 3$) mixture, $(NO–CO)_g$, through the blank IR reactor cell shows gas phase CO bands at 2176 and 2117 cm^{-1} and gas phase

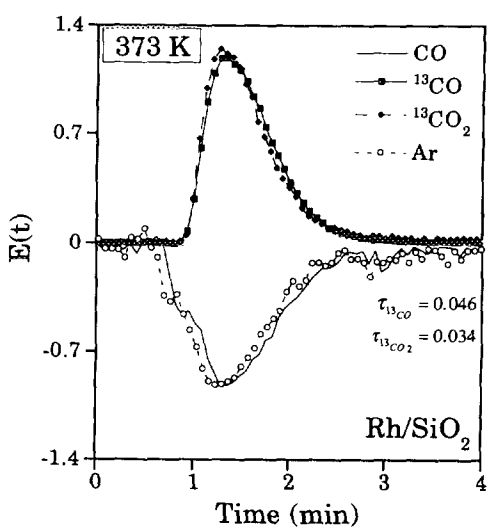

FIG. 9. MS analysis during steady-state isotopic analysis of NO–CO reaction on reduced Rh/SiO_2 at 373 K ($NO : CO : He = 1 : 1 : 3$).

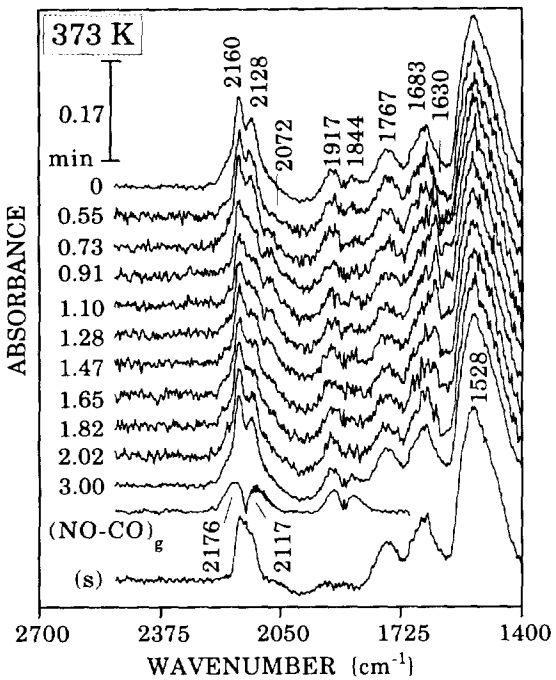

FIG. 10. IR spectra during steady-state isotopic analysis of NO–CO reaction on reduced Rh/SiO_2 at 373 K. $(NO–CO)_g$ denotes gas-phase NO–CO–He (1 : 1 : 3) spectrum in the blank reactor; (s) denotes spectrum at 3 min $(NO–CO)_g$ spectrum.

NO bands at 1916 and 1844 cm^{-1} and these bands are overlapped with CN, linear CO, and nitrosyl bands during the isotopic pulse transient on the catalyst. The difference spectrum(s) in Fig. 10 clearly shows that adsorbed NO^+ is present on the Rh/SiO_2.

Pulsing ^{13}CO into the ^{12}CO flow resulted in a downward shift in the wavenumber of the band at 2128 cm^{-1} to 2072 cm^{-1} that can be ascribed to the *R* branch of ^{13}CO, followed by an immediate shift back to the original wavenumber. The change in the 2128 cm^{-1} band is complicated by its downward shift and the possible contribution from the ^{13}CN band. The intensity of the CN band at 2160 cm^{-1} decreased about 14% before returning to its original intensity. Comparison of the IR spectra between 2050 and 2190 cm^{-1} before and during the pulse suggests that the CO species exhibiting the 2128 cm^{-1} band did not exchange with gaseous ^{13}CO completely. The incomplete exchange could be due to the low residence time of gaseous ^{13}CO in the reactor and slow rate of adsorption and desorption of CO exhibiting the 2128 cm^{-1} band. Larger volumes of ^{13}CO might be required to obtain a complete exchange of the adsorbed ^{12}CO by ^{13}CO during the isotopic pulse study. The band at 1630 cm^{-1} is due to a species containing C since the variation of the wavenumber and intensity of the band corresponds to the dynamics of the ^{13}CO pulse. The specific nature of the species remained unclear. No changes were observed in the intensities or wavenumbers of the nitrosyl bands.

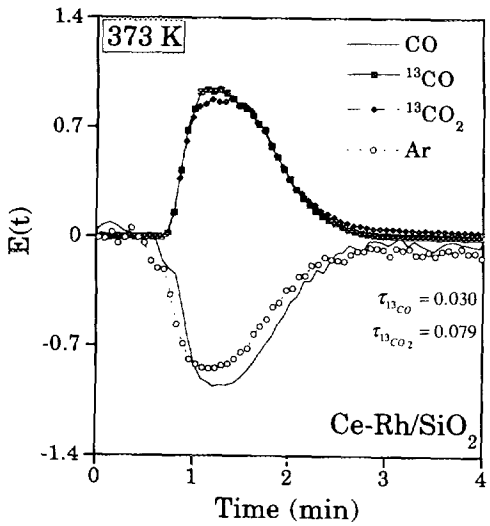

FIG. 11. MS analysis during steady-state isotopic analysis of NO–CO reaction on reduced $Ce–Rh/SiO_2$ at 373 K (NO : CO : He = 1 : 1 : 3).

Figure 11 shows the normalized MS response, $E(t)$, during the isotopic pulse study on $Ce–Rh/SiO_2$ at 373 K. The responses of gaseous reactants and products are similar to those observed on Rh/SiO_2. Comparison of the MS response on the Rh/SiO_2 and $Ce–Rh/SiO_2$ catalysts showed that Ce decreased $\tau_{^{13}CO}$ and increased $\tau_{^{13}CO_2}$ on Rh/SiO_2 at 373 K. Figure 12 shows the transient IR spectra

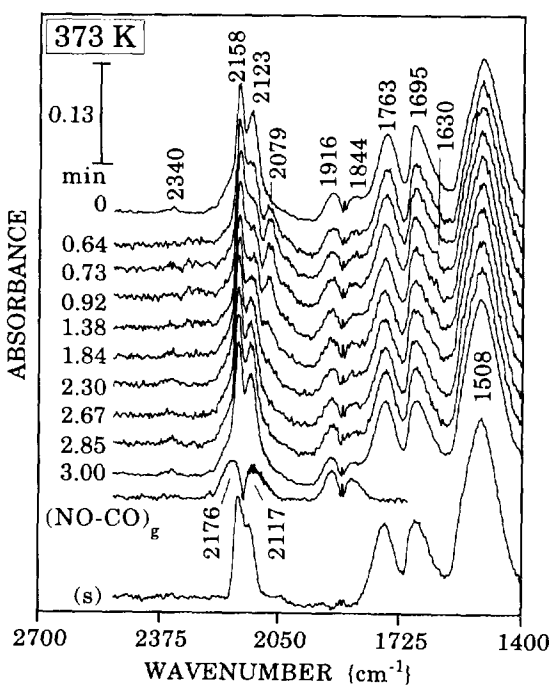

FIG. 12. IR spectra during steady-state isotopic analysis of NO–CO reaction on reduced $Ce–Rh/SiO_2$ at 373 K. $(NO–CO)_g$ denotes gas-phase NO–CO–He (1 : 1 : 3) spectrum in the blank reactor; (s) denotes spectrum at 3 min $(NO–CO)_g$ spectrum.

during the isotopic pulse investigation on Ce–Rh/SiO_2. The IR spectrum obtained before pulsing ^{13}CO showed the following bands: (i) a prominent CN band at 2158 cm^{-1}, (ii) a prominent linear CO band on Rh^{2+} at 2123 cm^{-1}, (iii) a NO^+ band at 1916 cm^{-1}, (iv) bands due to NO^- at 1763 and 1695 cm^{-1}, and (v) a band attributed to bidentate nitrato species at 1508 cm^{-1}, and weak CO_2 bands in the 2330–2360 cm^{-1} range. Pulsing ^{13}CO into ^{12}CO flow resulted in a downward shift in the linear CO band at 2123 cm^{-1} to 2079 cm^{-1}, followed immediately by an upward shift back to its original wavenumber. The decrease in the intensity of the 2123 cm^{-1} band and the increase in the intensity of the 2079 cm^{-1} band are more pronounced than those of their counterparts on Rh/SiO_2. The cause for the variation in the intensity and wavenumber of the 1630 cm^{-1} band remains unknown. There were no changes in the intensities or wavenumbers of the other bands that are related to adsorbed NO.

DISCUSSION

Adsorption of NO on reduced Rh/SiO_2 and Ce–Rh/SiO_2 at 298 and 373 K resulted in the formation of NO^+, a high wavenumber (1740–1770 cm^{-1}) and a low wavenumber (1650–1700 cm^{-1}) NO^- species, and bidentate nitrato species. The intensity of the NO^+ band was enhanced by Ce, as shown in Figs. 5 and 6; this may be attributed to the presence of Rh^+ associated with Ce. One major effect of Ce on the Rh surface was to inhibit the reductive agglomeration of Rh^+ to Rh^0 crystallite in a CO atmosphere at 298–473 K (17). No distinction in reactivity has been made in prior literature between the low wavenumber NO^- species and high wavenumber NO^- species. Studies of the interaction of adsorbed CO with gaseous NO reveal that gaseous NO preferentially adsorbs on a low wavenumber NO^- site and displaces linear CO from the reduced Rh site. Adsorption of NO as NO^- leading to desorption of linear CO suggests that the low wavenumber NO^- may adsorb on the reduced Rh site that chemisorbs linear CO. The lack of NO^- formation on the oxidized Rh surface in Fig. 4 further supports the suggestion that the reduced Rh site chemisorbs NO^-. The low N–O stretching frequency has been suggested to be an indication of the weakening of the N–O bond and the strengthening of the Rh–N bond (12, 25). As a result, the low wavenumber NO^- (1650–1700 cm^{-1}) should be more strongly bonded to the Rh surface than the high wavenumber NO^- species (1740–1770 cm^{-1}).

The high wavenumber NO^- species developed at 373 K following exposure of adsorbed CO to a 0.1 MPa NO flow and desorption of most adsorbed CO. The high wavenumber NO^- was not formed during the exposure of adsorbed ^{13}CO to NO at 423 K. Temperature-programmed NO–CO reaction has also revealed that the high wavenumber NO^- species is observed from 303 to 553 K, while the low wavenumber NO^- species is present from 303 to 493 K (48). The lack of high wavenumber NO^- formation at high temperature conditions further supports the weak bonding nature of the high wavenumber NO^- species compared to the low wavenumber NO^- species.

The low wavenumber NO^- species with a weakened N–O bond may have a high propensity to dissociate. Dissociation of adsorbed NO and the subsequent reaction between Rh–O and NO would lead to the formation of

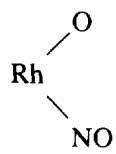

which is denoted as NO^+ (27). NO^+ can also be formed directly from NO adsorption on Rh^+ sites. In the present study, prolonged exposure of adsorbed CO to gaseous NO led to the formation of gaseous N_2O, adsorbed NO^+, and bidentate nitrato species with the removal of bridged CO and tilted CO on the Rh^0 site. The removal of the bridged CO and tilted CO can be attributed to the oxidation of the Rh surface by the dissociation of adsorbed NO. The N from the dissociated NO reacts with adsorbed NO to form gaseous N_2O as shown in Figs. 1 and 3. The absence of CO_2 during the interaction of adsorbed CO with gaseous NO at 373 K can be attributed to the desorption of adsorbed Co before NO dissociation. Figures 1 and 3 show that N_2O, the product of NO dissociation, was formed after all the CO desorbed.

Interaction of preadsorbed NO with gaseous CO showed that the CO did not displace the adsorbed NO^- at 298 and 373 K on Rh/SiO_2 and Ce–Rh/SiO_2 indicating that adsorbed NO^- is more strongly bonded than adsorbed CO on the Rh/SiO_2 surface. Prolonged exposure of preadsorbed NO to gaseous CO led to the displacement of NO^+ at 373 K and to the gradual formation of the gem-dicarbonyl and linear CO on Rh^+ sites. The result suggests that the NO^+ weakly adsorbed on the Rh^+ sites allows the CO to displace a fraction of adsorbed NO^+ to form the gem-dicarbonyl. The NO^+ and gem-dicarbonyl may occupy the same Rh^+ site. The linear and bridged CO were not formed since the reduced Rh sites strongly chemisorb NO^-. The absence of CO_2 during the interaction of adsorbed NO with gaseous CO is a result of the lack of NO dissociation. The gem-dicarbonyl formed from the displacement of the NO^+ by CO is not able to react with the adsorbed oxygen at 373 K. The gem-dicarbonyl showed little reactivity toward 0.1 MPa of O_2 on Rh/SiO_2 at 358 K (16). Temperatures above 448 K are required for the removal of the adsorbed oxygen by reductive agglomeration to form CO_2 and linear CO from the gem-dicarbonyl in the presence of 50 Torr CO (49).

CO-induced reductive agglomeration and oxidative dis-

ruption have been extensively studied by Solymosi and co-workers (12, 17, 28, 49). In contrast to the reductive agglomeration at temperatures above 448 K, CO can induce oxidative disruption of reduced Rh crystallites at low temperatures, resulting in the formation of gem-dicarbonyl. NO can further accelerate the process of oxidative disruption of Rh crystallites and hinder the reductive agglomeration at temperatures above 448 K. The rapid development of gem-dicarbonyl following pulsing CO over preadsorbed NO on the reduced Rh and Ce–Rh catalysts as shown in Figs. 5 and 6 further confirms the role of NO in promoting oxidative disruption of Rh crystallites (28).

The difference in the reactivity of the adsorbed species in the presence of gaseous CO, NO, and NO–CO gases may be explained in terms of the effects of the gaseous reactants on the coverage of adsorbed species and the surface state of the catalyst. Infrared spectra of steady-state NO–CO (1 : 1) reaction at 373 K reveal that the surface states of Rh/SiO_2 (Fig. 10) and $Ce–Rh/SiO_2$ (Fig. 12) under a NO–CO environment are different from those observed under an NO or CO environment. The partial pressure of NO and CO also appears to affect the adsorbed species and surface state of the catalyst. Gem-dicarbonyl and weakly adsorbed NO were detected on the 2% Rh/Al_2O_3 catalyst under a mixture of 1 Torr (0.13 KPa) NO and 10 Torr (1.3 KPa) CO at 300 K (28). The dominant species on the catalyst during the NO–CO reaction at 373 K and 20 KPa NO and 20 KPa CO on Rh/SiO_2 and $Ce–Rh/SiO_2$ in the present study are NO^-, bidentate nitrato species, adsorbed CN, and a linear CO species exhibiting the 2128 and 2123 cm^{-1} bands. The active surface at 373 K did not chemisorb CO as linear CO and bridged CO on the Rh^0 site and gem-dicarbonyl on the Rh^+ site, suggesting that CO primarily adsorbs on Rh^{2+} sites while NO primarily adsorbs on the reduced Rh site to form NO^-. The role of adsorbed CO on Rh^{2+} sites in CO_2 formation remains unclear due to incomplete exchange between this CO with gaseous ^{13}CO. Comparison of the IR spectra during NO–CO reaction on Rh/SiO_2 and $Ce–Rh/SiO_2$ shows that the addition of Ce to the Rh/SiO_2 catalyst resulted in an increase in the ratio of intensity of the high wavenumber (1763 and 1765 cm^{-1}) to low wavenumber (1683 and 1695 cm^{-1}) NO^- bands. Tilted CO chemisorbed on the reduced Rh site is not present in an NO–CO atmosphere since the reduced Rh sites are occupied by chemisorbed NO as NO^-.

The mechanism of CO_2 formation on a 4.6% Rh/SiO_2 catalyst during the NO–CO reaction has been proposed to involve the decomposition of NO followed by reaction of the adsorbed oxygen with CO to form CO_2 at 463–523 K (25). The rate-limiting step for CO_2 formation has been proposed to be the decomposition of NO to form surface N and O atoms at NO conversions of less than 50% (25). The isotopic pulse on Rh/SiO_2 at 373 K in this study also supports this mechanism. The reaction scheme for CO_2 formation from CO is shown below:

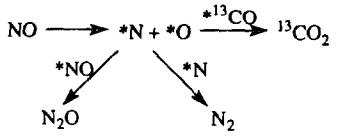

* denotes adsorbed species

The response of $^{13}CO_2$ almost coincides that of ^{13}CO (Figs. 9 and 11) indicating that the reaction of adsorbed ^{13}CO with surface oxygen is rapid. Therefore, the rate-limiting step may be associated with the dissociation of NO. The dynamic nature of NO dissociation has to be investigated by isotopic NO pulse or step transient methods.

The rate of CO_2 formation from the NO–CO reaction depends on not only the surface state of the catalyst but also on the coverage of adsorbed species. It is difficult to accurately determine the concentration of adsorbed species during different runs by IR intensity because of the use of different catalyst disks with slightly varying thicknesses. The wavenumber of adsorbed NO^- species increases with its concentration. The extent of upward shift in the wavenumber can be used as a qualitative measure of the surface concentration, provided that dipole–dipole interaction between the adsorbed species is a dominant factor affecting the wavenumber of adsorbed NO. The increase in the wavenumber of both high-wavenumber (1767 and 1763 cm^{-1}) and low-wavenumber (1683 and 1695 cm^{-1}) NO^- species during steady-state NO–CO reaction (Figs. 10 and 12) compared to the wavenumber observed during the pulse studies (Figs. 1, 3, 5, and 6) indicates that the concentration of the chemisorbed NO^- is significantly greater during the steady-state NO–CO reaction than during the pulse studies.

NO dissociation is a function of particle size and support composition (50). Large particle sizes such as the Rh particles in this study favor NO dissociation (50). NO temperature-programmed desorption (TPD) studies have also revealed that increasing NO coverage increases the ratio of low temperature N_2 formation peak to the high temperature N_2 formation peak (51). High coverage of NO should facilitate NO dissociation at low temperature. Although the presence of CO may complicate NO dissociation, the formation of CO_2 may be related to the dissociation of NO under high coverage condition in the presence of gaseous NO and CO. The exact nature of how the coverage affects the reactivity remains to be investigated.

The surface state of Rh catalyst strongly depends on the gaseous environment and reaction conditions (28, 40, 41). This study demonstrates that the adsorption characteristics of individual reactants vary with the gaseous environments. Therefore, our observation at 298–373 K cannot be extended to high temperature conditions of three-way catalysts. The study does provide valuable insight

into the behavior of multiple and reactive adsorbates on noble metal surfaces.

CONCLUSIONS

The reactivity of adsorbed CO and NO depends on the surface state of the catalyst and reaction conditions. Adsorbed CO on the reduced Rh/SiO_2 and $Ce–Rh/SiO_2$ is not able to react with a gaseous NO pulse to form CO_2 at 303–423 K. NO adsorbs as a low wavenumber NO^- species on the Rh^0 site resulting in the desorption of linear CO on the Rh^0 site. Both linear CO and NO^- may chemisorb on the same Rh^0 site. Long NO exposure led to the complete desorption of bridged CO on Rh/SiO_2, and tilted CO on the $Ce–Rh/SiO_2$ and adsorption of NO as NO^+, high wavenumber NO^-, and bidentate nitrato species. Linear CO on Rh/SiO_2 was found to exchange with gaseous ^{13}CO at a higher rate than bridged CO. The oxidized Rh surface failed to chemisorb NO even after exposure at 298–373 K and 0.1 MPa of NO for an extended period of time.

Gaseous CO cannot displace preadsorbed NO^- during the pulse experiments; prolonged exposure of preadsorbed NO to CO, however, resulted in the displacement of NO^+ by CO leading to chemisorption of CO as gem-dicarbonyl and a linear CO on Rh^+. The presence of both NO and CO gases led to increase in the coverage of NO^- and adsorption of CO on Rh^{2+} sites and promoting the formation of CO_2. The surface state of the active catalyst catalyzing the formation of CO_2 is different from that of the catalyst chemisorbing the NO and CO reactants individually. The adsorption characteristics of individual CO and NO are not the same as those of adsorbed CO and NO under conditions where both reactants are present.

ACKNOWLEDGMENT

G.S. and S.D. are grateful for the financial support from the Department of Chemical Engineering at the University of Akron.

REFERENCES

1. Funabiki, M., Yamada, T., Kayano, K., *Catalysis Today*, **10,** 33 (1981).
2. Briggs, W. S., *in* "Applied Industrial Catalysis" (B. E. Leach, Ed.) Vol. 3, Academic Press, New York, 1984.
3. Cooper, B. J. Evans, W. D. J., and Harrison, B., *in* "Catalysis and Automotive Pollution Control" (A. Crucq and A. Frennet, Eds.), Vol. 30, p. 117. Elsevier, New York, 1987.
4. Oh, S. H., Fisher, G. B., Carpenter, J. E., and Goodman, D. W., *J. Catal.* **100,** 360 (1986).
5. Hahn, T., and Lintz, H. G., *Surf. Sci.* **211,** 1030 (1988).
6. Farrauto, R. J., Heck, R. M., and Speronello, B. K., *Chem. Eng. News*, **7,** 34 (1992).
7. Taylor, K. C., *Catal. Rev. Sci. Eng.* **35**(4), 457 (1993).
8. Yang, A. C., and Garland, C. W., *J. Phys. Chem.* **61,** 1504 (1957).
9. Yates, J. T. Jr., Duncan, T. M., Worley, S. D., and Vaughan, R. W., *J. Chem. Phys.* **70,** 1219 (1979).
10. Yates, J. T. Jr., Duncan, T. M., and Vaughan, R. W., *J. Chem. Phys.* **71,** 3908 (1979).
11. Rice, C. A., Worley, S. D., Curtis, C. W., Guin, J. A., and Tarrer, A. R., *J. Chem. Phys.* **74,** 6487 (1981).
12. Novak, E., and Solymosi, F., *J. Catal.* **125,** 112 (1990).
13. Konishi, Y., Ichikawa, M., and Sachtler, W. M. H., *J. Phys. Chem.* **91,** 6286 (1987).
14. Kesroui, S., Oukaci, R., and Blackmond, D. G., *J. Catal.* **105,** 432 (1987).
15. Underwood, R. P., and Bell, A. T., *J. Catal.* **111,** 325 (1988).
16. Li, Y. E., and Gonzales, R. D., *J. Phys. Chem.* **92,** 1589 (1988).
17. Solymosi, F., Pasztor, M., and Rakhely, G., *J. Catal.* **110,** 413 (1988).
18. Chuang, S. S. C., and Pien, S. I., *J. Mol. Catal.* **55,** 12 (1989).
19. Chuang, S. S. C., and Pien, S. I., *J. Catal.* **135,** 618 (1992).
20. Chuang, S. S. C., and Pien, S. I., *J. Catal.* **138,** 536 (1992).
21. Chuang, S. S. C., Srinivas, G., and Mukherjee, A., *J. Catal.* **139,** 490 (1993).
22. Srinivas, G., and Chuang, S. S. C., *J. Catal.* **144,** 131 (1993).
23. Arai, H., and Tominaga, H., *J. Catal.* **43,** 131 (1976).
24. Solymosi, F., and Sarkany, J., *Appl. Surf. Sci.* **3,** 68 (1979).
25. Hecker, W. C., and Bell, A. T., *J. Catal.* **84,** 200 (1983).
26. Hecker, W. C., and Bell, A. T., *J. Catal.* **85,** 389 (1984).
27. Hyde, E. A., Rudham, R., and Rochester, C. H., *J. Chem. Soc. Faraday. Trans. 1* **80,** 531 (1984).
28. Solymosi, F., Bansagi, T., and Novak, E., *J. Catal.* **112,** 183 (1988).
29. Dictor, R., *J. Catal.* **109,** 89 (1988).
30. Srinivas, G., Chuang, S. S. C., and Debnath, S., *in* "Environmental Catalysis" (J. N. Armor, Ed.), ACS Symposium Series, Vol. 552, p. 158. Am. Chem. Soc., Washington, DC, 1994.
31. Gandhi, H. S. Piken, A. G. Shelef, M., and Delosh, R. G., Paper No. 760201. *SAE*, 1976.
32. Hindin, S. G., *U.S. Patent* 3,870,455, 1973.
33. Weibel, M., Garin, F., Bernhardt, P., Marie, G., and Prigent, M., *in* "Catalysis and Automotive Pollution Control II" (A. Crucq, Ed.), p. 195. Elsevier, Amsterdam, 1991.
34. Oh, S., *J. Catal.* **124,** 477 (1981).
35. Fisher, G. B., Theis, J. R., Casarella, M. V., and Mahan, S. T., Paper No. 931034. *SAE*, 1993.
36. Yamada, T., Onishi, T., and Tamaru, K., *Surf. Sci.* **157,** L389 (1985).
37. Winslow, P., and Bell, A. T., *J. Catal.* **86,** 154 (1984).
38. Akhter, S., and White, J. M., *J. Vac. Sci. Technol. A* **6**(3), 864 (1988).
39. Shido, T., and Iwasawa, Y., *J. Catal.* **141,** 71 (1993).
40. Krause, K. R., and Schmidt, L. D., *J. Catal.* **140,** 424 (1993).
41. Chojnacki, T., Krause, K. R., and Schmidt, L. D., *J. Catal.* **128,** 161 (1991).
42. Hindermann, J. P., Hutchings, G. J., and Kiennemann, A., *Catal. Rev. Sci. Eng.* **53**(1), 1 (1993).
43. Srinivas, G., Chuang, S. S. C., and Balakos, M. W., *AIChE J.* **39,** 530 (1993).
44. *The Standard Sadtler Spectra*. Sadtler Research Laboratories, Philadelphia, 1967.
45. Rasko, J., and Solymosi, F., *J. Chem. Soc. Faraday Trans. 1* **76,** 2383 (1980).
46. Debnath, S., M. S. Thesis, the University of Akron, 1993.
47. Fogler, H. S., "Elements of Chemical Reaction Engineering," Prentice–Hall, Englewood Cliffs, NJ, 1992.
48. Srinivas, G., Ph.D. Dissertation, the University of Akron, 1994.
49. Solymosi, F., and Bansagi, T., *J. Phys. Chem.* **97,** 10133 (1993).
50. Zafiris, G., Roberts, S. I., and Gorte, R. J., *in* "Catalytic Control of Air Pollution" (R. G. Silver, J. E. Sawyer, and J. C. Summers, Eds.), ACS Symposium Series, Vol. 495, p. 73. Am. Chem. Soc., Washington, DC, 1992.
51. Chin, A. A., and Bell, A. T., *J. Phys. Chem.* **87,** 3700 (1983).